

# Optical Induction and Erasure of Ferroelectric Domains in Tetragonal PMN-38PT Crystals

Xin Chen, Dawei Liu, Shan Liu, Leszek M. Mazur, Xin Liu, Xiaoyong Wei, Zhuo Xu, Junli Wang,\* Yan Sheng,\* Zhiyi Wei, and Wieslaw Krolikowski

PT-relaxor ferroelectrics exhibit excellent piezoelectric and quadratic nonlinear optical properties, making them prominent candidates for realization of phononic and nonlinear photonic crystals which rely on spatially patterned ferroelectric domains. However, formation of domain patterns, especially in three dimensions, has been challenging. This paper presents the first experimental demonstration of localized ferroelectric domains and their 2D and 3D patterns inside  $0.62\text{Pb}(\text{Mg}_{1/3}\text{Nb}_{2/3})\text{O}_3\text{-}0.38\text{PbTiO}_3$  (PMN-38PT) single-domain crystals engineered with focused near-infrared femtosecond laser pulses. Two types of domains are optically induced. Primary domains are formed in the focal volume of the beam, and secondary domains appearing at higher laser power, in the shape of hollow cylindrical structures, are formed around the beam. A physical mechanism of optical domain inversion involving thermoelectric and space charge fields is proposed. This study contributes to a deeper understanding of domain formation and structuring in PMN-PT relaxor-based ferroelectrics, paving the way to integrate electromechanical, acoustic, and nonlinear optical effects in a single crystal.

Furthermore, they show extremely high electro-optic (EO) and acousto-optic (AO) coefficients.<sup>[2]</sup> Recent studies of quadratic nonlinearity of  $\text{Pb}(\text{Mg}_{1/3}\text{Nb}_{2/3})\text{O}_3\text{-PbTiO}_3$  (PMN-PT) crystals in powder form indicated their potential for nonlinear optics.<sup>[3]</sup> Because of these excellent properties, the relaxor-based ferroelectric crystals could be of great interest as piezoelectric phononic crystals (PPCs) or acoustic superlattices (ASLs) to confine and manipulate phonons for a wide range of applications, including acoustic filters, noise isolation, and heat managements.<sup>[4]</sup> Unlike the pure elastic phononic crystal, which usually consists of materials with different elastic moduli and/or mass densities,<sup>[5]</sup> the domain inversion phononic crystal (DIPC) is a monolithic entity within the single ferroelectric, making it more attractive in applications like surface acoustic wave (SAW) devices.<sup>[4a,b,6]</sup> Similarly, ferroelec-

trics with spatially modulated second-order optical nonlinear susceptibility  $\chi^{(2)}$ , also known as nonlinear photonic crystals (NPCs) or optical super lattices (OSLs), can be used to generate, shape, and manipulate optical waves at new frequencies<sup>[7]</sup> by utilizing the so called quasiphase matching (QPM).<sup>[8]</sup> However, the

## 1. Introduction


Among the large family of ferroelectric materials, the PT-relaxor crystals stand out because of their giant piezoelectric constants and ultrahigh electromechanical coupling properties.<sup>[1]</sup>

X. Chen, J. Wang  
School of Physics and Optoelectronics Engineering  
Xidian University  
Xi'an 710071, China  
E-mail: wangjunli@mail.xidian.edu.cn

D. Liu, S. Liu, Y. Sheng, W. Krolikowski  
Laser Physics Centre, Research School of Physics  
Australian National University  
Canberra, ACT 0200, Australia  
E-mail: yan.sheng@anu.edu.au

L. M. Mazur, W. Krolikowski  
Science Program  
Texas A&M University at Qatar  
Doha 23874, Qatar

L. M. Mazur  
Advanced Materials Engineering and Modelling Group  
Faculty of Chemistry  
Wroclaw University of Science and Technology  
Wyb. Wyspianskiego 27, Wroclaw 50-370, Poland

 The ORCID identification number(s) for the author(s) of this article can be found under <https://doi.org/10.1002/adom.202102115>.

X. Liu, X. Wei, Z. Xu  
Electronic Materials Research Laboratory  
Key Laboratory of the Ministry of Education and International Center for Dielectric Research  
Xi'an Jiaotong University  
Xi'an 710049, China

Y. Sheng  
Laboratory of Infrared Materials and Devices  
Research Institute of Advanced Technologies  
Ningbo University  
Ningbo, Zhejiang 315211, China

Z. Wei  
Beijing National Laboratory for Condensed Matter Physics  
Institute of Physics  
Chinese Academy of Sciences  
Beijing 100190, China

DOI: 10.1002/adom.202102115

above-mentioned applications require spatially patterned ferroelectric domains from 1 to 3 dimensions. Traditional domain engineering in ferroelectrics relies on the electric field poling (EFP), which produces domain structures through patterned electrodes biased with high external voltage along crystal's polar axis.<sup>[9]</sup> Hence, this approach does not permit to create isolated inverted domains and their 3D spatial patterns. The EFP may also cause cracking of relaxor-based ferroelectrics due to the large electric field induced strain<sup>[10]</sup> and appearance of unexpected domains structures such as the 90° domain walls.<sup>[11]</sup> So far, the EFP has been used to create single domain bulk PMN-PT relaxor-based ferroelectric samples. In very recent works, the electron beam poling (EBP) was successfully employed to create simple domain structures.<sup>[12]</sup> However, no individual domains or their structures located inside the crystal could be realized with this technique. Furthermore, EBP requires sophisticated equipment which drastically limits its practicality.

Very recently, the formation of isolated ferroelectric domains and creation of fully 3D domain patterns became possible thanks to a breakthrough approach based on domain inversion by using femtosecond laser direct writing.<sup>[13]</sup> The process involves the nonlinear absorption of tightly focused near infrared (NIR) femtosecond laser pulses and subsequent fast heating of the crystal. The high temperature gradient induces a thermoelectric field which can invert the spontaneous polarization and create localized domain in the focal region.<sup>[14]</sup> This pulsed laser domain inversion (or laser poling) technique has been used in fabrication of 2D and 3D domain structures in multidomain crystals like Ba<sub>0.77</sub>Ca<sub>0.23</sub>TiO<sub>3</sub> (BCT), as-grown Ca<sub>0.28</sub>Ba<sub>0.72</sub>Nb<sub>2</sub>O<sub>6</sub> (CBN) and Sr<sub>0.75</sub>Ba<sub>0.25</sub>Nb<sub>2</sub>O<sub>6</sub> (SBN),<sup>[13,15]</sup> as well as in monodomain crystals like LiNbO<sub>3</sub> and uniformly poled CBN crystals.<sup>[14,16]</sup> In all these cases, the inverted ferroelectric domains were exactly within the focal region of the writing laser pulses.

In this paper, we present the first experimental demonstration of 3D spatially localized domain inversions inside single domain tetragonal 0.62Pb(Mg<sub>1/3</sub>Nb<sub>2/3</sub>)O<sub>3</sub>-0.38PbTiO<sub>3</sub> (PMN-38PT) crystal as a representative for PT-relaxor ferroelectrics. By focusing IR femtosecond laser pulses inside the crystal, the fully 3D inverted ferroelectric domain structures could be created at arbitrary location. Spatially localized, finite size ferroelectric domains can be formed in the laser focal region without any damages to the medium. Interestingly, we discovered that under certain conditions domains can be inverted not only in the focal region but also outside of this region, resulting in complex, but fully controlled, domain morphology. Furthermore, we have written inverted domains that are close to each other, and found that the already induced donut-shaped peripheral domain can be erased by the newly formed domain in the overlapping areas. Our results thus open up possibility to develop a class of hybrid devices combining the excellent piezoelectric and optical properties of PT-relaxor-based ferroelectric crystals.

## 2. Results and Discussion

### 2.1. Morphology of 3D Domains Inside Single-Domain Crystal

The single-domain crystals used for 3D localized domain inversions were [001]-oriented (or z-cut), electrically poled tetragonal

PMN-38PT crystals, as shown in Figure S1 in the Supporting Information. More details on crystal growth, single-domain fabrication, and 3D laser poling can be found in the Experimental Section. To identify and visualize inverted domains inside the crystals, we used Čerenkov second harmonic microscopy (ČSHM) which is a nondestructive diagnostic technique that can provide 3D imaging with submicron resolution.<sup>[17]</sup> Strong Čerenkov second harmonic (ČSH) can be detected from boundaries of  $\chi^{(2)}$  regions, such as domain walls. Unlike SH generated inside uniform region which is collinear with the fundamental beam, the ČSH is emitted in transverse direction, allowing its easy detection. Therefore, the  $\chi^{(2)}$  domain patterns can be visualized by analyzing the ČSH signal collected by scanning the focused laser beam in the crystal. The 3D images of domain structures are produced by stacking *xoy* images recorded in the whole depth range (*z*) of the structures using the ImageJ software. In addition, domain reversal was independently verified by using piezoresponse force microscopy (see Figure S2 in the Supporting Information for details).

Figure 1 depicts the example of 3D localized ferroelectric domain structure formed entirely inside of the z-cut PMN-38PT crystal. The structure was created by illuminating the sample with focused 800 nm laser beam of 250 mW of average power. The focus of the beam was located deep inside the medium. After writing the bottom layer the sample was translated along the [001] direction and then the second layer of domain pattern was written. Repeating the procedure resulted in the full 3D structure being completely immersed inside of the sample. In the example shown in Figure 1, the shallowest layer is located 192  $\mu\text{m}$  below the surface. The structure consists of seven layers of domains arranged in a regular rectangular pattern in each layer with the period of 5–10  $\mu\text{m}$  along the *x* and *y* directions, respectively. The layers are separated by 24  $\mu\text{m}$  distance. As the inset shows, each subsequent layer is transversely shifted by 5  $\mu\text{m}$ . In this particular instance, each domain was created by illuminating the corresponding position in the crystal with the laser beam over 250 ms. In the next step, the laser beam was turned off and the sample was translated to a new location. Process was repeated until the whole 3D pattern was created. As graph in Figure 1 shows, the individual domains have elongated shape of roughly 20–25  $\mu\text{m}$  long. The diameter of the domains is between 2 and 3  $\mu\text{m}$ , which is comparable with the size of focus spot using objective lens with numerical aperture (NA) of 0.4. Using current laser writing conditions without compensating for the aberrations of the poling beam, the deepest laser induced domains are located some 480  $\mu\text{m}$  inside, which is roughly half the thickness of the crystal.

We found that the laser beam can directly write domains inside single-domain PMN-PT no matter it irradiates the crystal from +*z* or –*z* surfaces. Therefore, it is possible to inscribe 3D domain structures at any depths inside even thick crystals, which can maximize the potential of PMN-PT in both acoustic and nonlinear optical applications.

Domain inversion process described above appears to be very reliable and repeatable. It can be accomplished at different depths inside the crystal (even hundreds of  $\mu\text{m}$ ) and for input average power ranging from 230 up to 260 mW. Furthermore, the process works for shorter wavelength as well. In some of our experiments we used 780 nm wavelength (see Figure S3

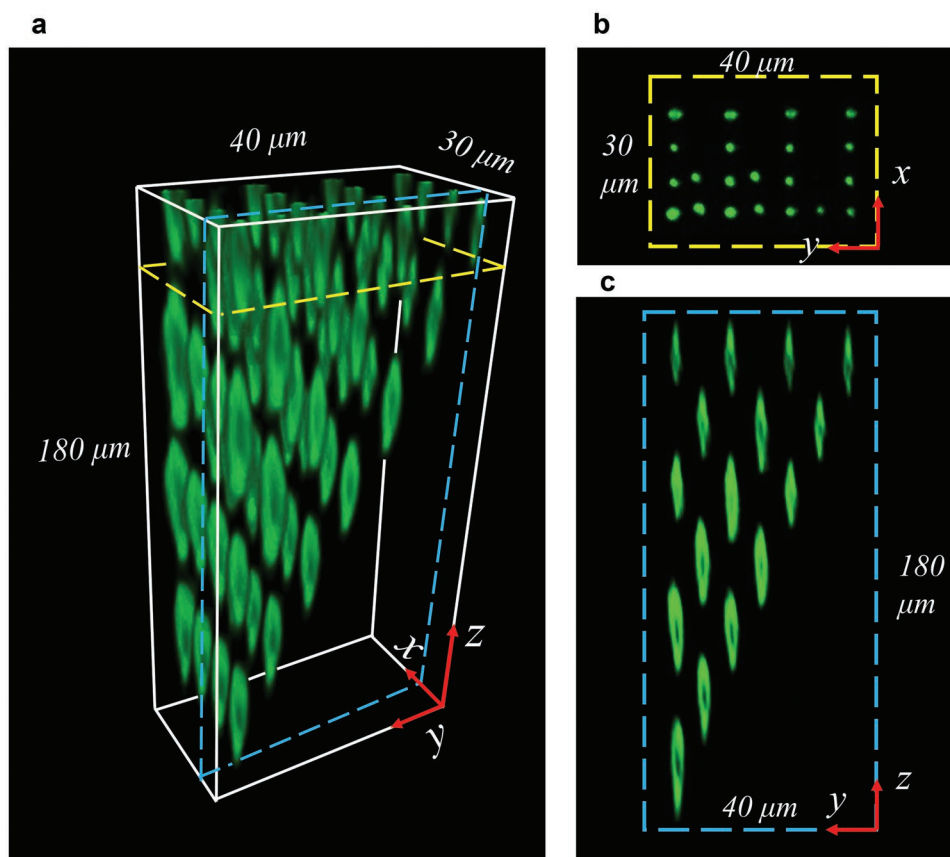


**Figure 1.** Optically induced ferroelectric domain patterns in a single-domain, tetragonal, and [001]-oriented PMN-38PT crystal. a) Čerenkov second harmonic microscopy (ČSHM) image of the 3D ferroelectric domain patterns inscribed with infrared ultrafast light beam from  $+z$  side of the crystal. The graphs of b) and c) depict corresponding cross-sections of the structure. The yellow and blue dotted-line boxes indicate the locations of the  $xy$  and  $yz$  cross-section views of the structure.

in the Supporting Information). In this case the threshold for domain inversion decreases as the nonlinear absorption which constitutes the foundation of the effect increases with shorter wavelengths. The upper power limit is imposed by the damage threshold of the crystal. Under our current experimental condition, the damage thresholds are 270 and 250 mW (192  $\mu\text{m}$  beneath the crystal surface) for the writing wavelengths of 800 and 780 nm, respectively.

Interestingly, we find that above certain power level (here 240 mW), the morphology of the created domains abruptly changes. Specifically, we observe that for sufficiently high light power two types of ferroelectric domains are simultaneously formed. The first one, which we call “primary” domains, are the domains described above and presented in Figure 1. They have a form of elongated, narrow structures, formed in the focal volume of the beam. The second type, “secondary,” form for the input power above 240 mW. They acquire a form of long, hollow cylinder with its axis coinciding with that of the laser beam. **Figure 2** depicts 3D ferroelectric domain pattern fabricated with laser power of 250 mW. The corresponding cross-sections of one row of the domains clearly reveal their intricate structure. The secondary domains can be seen as hollow cylinders with inner and outer radii of 5 and 7  $\mu\text{m}$ , respectively. It should be noticed that while the cylindrical symmetry of these

domains is fully preserved, their structure changes with depth. Initially the transverse cross-section has a clear donut shape but it breaks down into tiny islands deeper in the medium (middle row in Figure 2c). Finally at certain depth, the secondary domains completely disappear, leaving only primary, centrally located domains visible.

Dependence of experimentally determined diameter and length of primary and secondary domains, as a function of laser writing power is depicted in **Figure 3**. It is clearly seen the primary and secondary domains behavior differently with increasing laser power. The measured threshold for primary domain inversion is  $P = 230$  mW inside the single-domain PMN-38PT at 800 nm laser wavelength. At this power, the diameter of the primary domains is around 1  $\mu\text{m}$ , which is comparable with the size of the focal area of the beam. It then grows almost linearly with increasing writing power. At the same time the length of these domains remains basically constant just above 20  $\mu\text{m}$ . At input power  $P = 240$  mW, the secondary domains start to appear. With higher power, their transverse size and length grow quickly, reaching, almost 11 and 60  $\mu\text{m}$  at  $P = 250$  mW, respectively. Operation at even higher input laser power is prohibited because of the permanent laser damages to the crystal. As Figure 3 shows, from  $P = 240$  mW until  $P = 250$  mW both types of domains coexist.

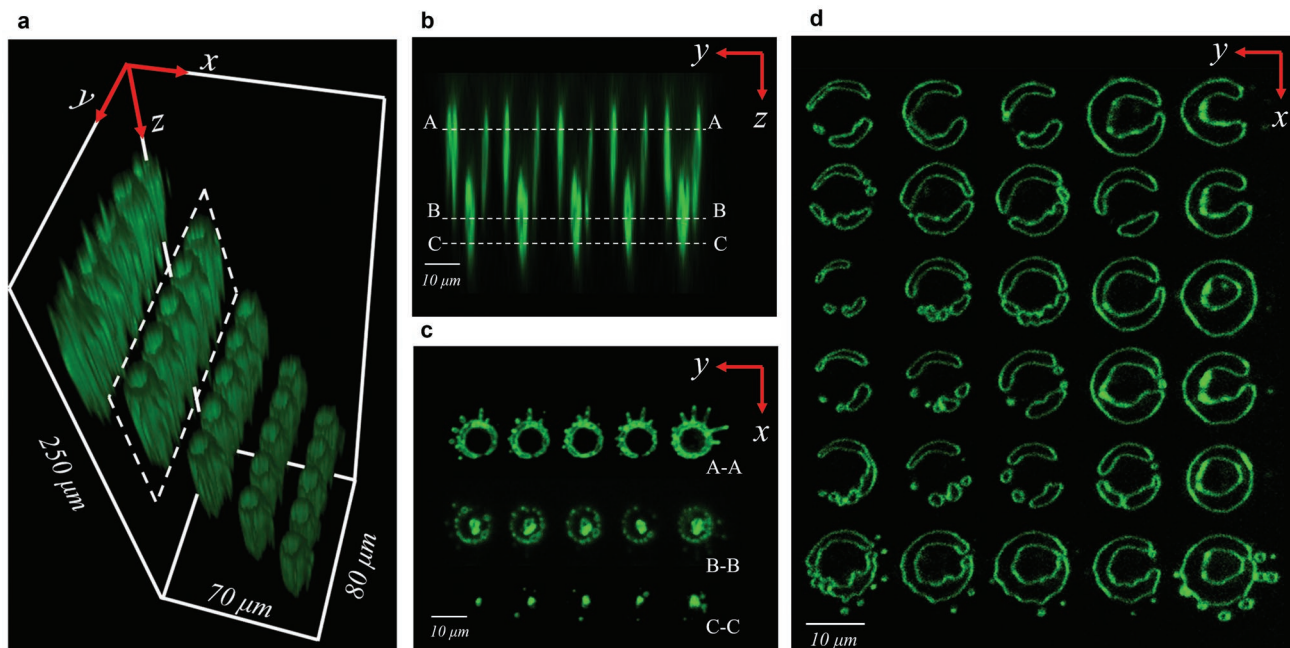


**Figure 2.** The laser induced primary and secondary ferroelectric domains in PMN-38PT. a)  $\check{C}$ SHM image of a group of these domains located at different depths inside a single-domain PMN-38PT crystal. The top layer is located 192  $\mu\text{m}$  below the negative  $z$  surface. b) The  $yoz$  cross-sectional view of a single domain row. c) Transverse  $xoy$  cross-sections of the domains at different depths. d) Another example of secondary domain pattern created with 800 nm laser beam. All domain structures were fabricated by illuminating the sample from  $-z$  surface.

It should be stressed that the formation of primary and secondary domains is a very repeatable process and takes place under various writing conditions. For instance, while the 3D domain pattern depicted in Figure 2 was created by focusing the 800 nm beam inside the crystal and simultaneously translating the focus 24  $\mu\text{m}$  along the polar ( $z$ ) axis, similar pattern forms in the stationary writing regime, when the focus of the laser beam remains in the same point during the illumination.

By creating linear sequences of inverted domains, we discovered that the originally formed secondary domain can be

partly erased by the newly formed domain if they both overlap. This effect is illustrated in Figure 4, which depicts a few linear periodic sequences of secondary domains fabricated with different separation ( $\Lambda$ ), at input power of  $P = 250$  mW. In each sequence the domains were written from left to right. We can see that with domain separation smaller than the diameter of the secondary domain (here  $\approx 10$   $\mu\text{m}$ ), the newly formed domain erases the right part of the preceding domain. This effect becomes even more pronounced at  $\Lambda \leq 2$   $\mu\text{m}$ . Every time a new domain is formed, it completely erases the right half of preceding domain. Repeating the process leads to the formation of the long U-shaped secondary domain, as seen in Figure 4b. We found that the laser erasure process is independent of the time interval between writing two neighboring secondary domains. A series of experiments with time interval ranging from 20 min up to 2 h were conducted (see Figure S5 in the Supporting Information). All the secondary domains in the overlapping region were erased in these experiments.

What is really striking about the secondary domains is their spatial location and direction of growth. First, they form away from the laser beam. The actual distance from the beam axis is roughly 3  $\mu\text{m}$  at the threshold power of 240 mW, and then increases almost linearly with the laser beam power (see Figure 3). Second, these domains originate at the crystal depth corresponding to the location of the beam focus, and then grow toward the  $-z$  surface of the crystal. We confirmed that this behavior is insensitive to the direction of the laser beam whether it propagates from positive or negative  $z$  surface. These features indicate that the formation of secondary domains must be governed by physical process different from that of the “primary” domains.

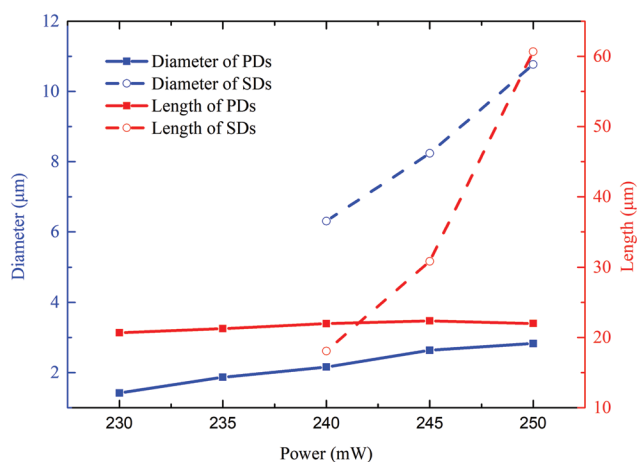


**Figure 3.** The average diameter (blue) and length (red) of primary domains (PDs) and secondary domains (SDs) as a function of the input power of the laser poling beam. Here, all the domains were inscribed using an 800 nm laser beam incident from the  $-z$  facet of the crystal. A detailed evolution of the domain morphology is shown in Figure S4 in the Supporting Information.

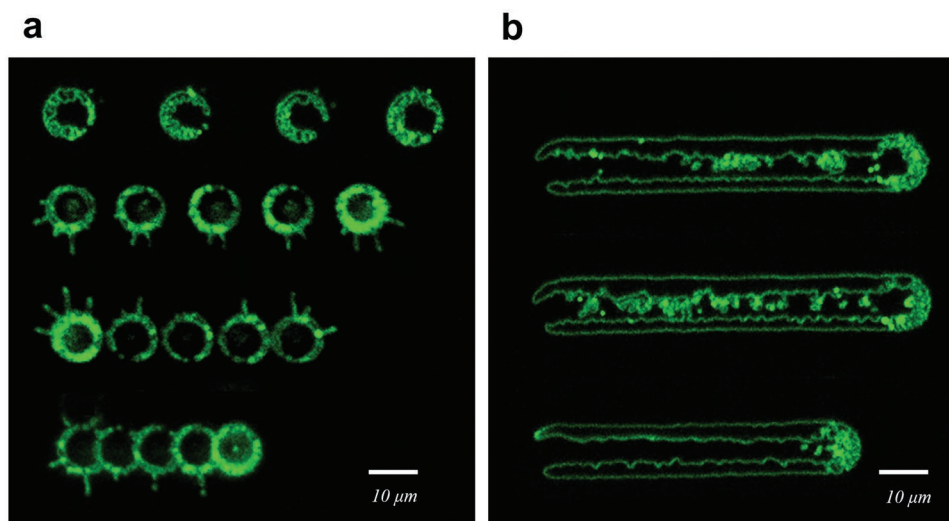


**Figure 4.** Laser erasure of secondary domains inside PMN-38PT. a) ČSHM images of secondary domains formed with separation distance  $\Lambda = 24, 15,$  and  $8 \mu\text{m}$ , from top to bottom, respectively. b) Linear secondary domain patterns formed for small domain separation along the writing direction. Specifically,  $\Lambda = 2 \mu\text{m}$  in the first two patterns and  $\Lambda = 1 \mu\text{m}$  in the last one.

## 2.2. Mechanism of 3D Laser Poling Inside PMN-38PT

We believe that the “primary” domains are formed thanks to temperature gradient-induced thermoelectric field which, when exceeds the coercive field, flips locally the spontaneous polarization of the crystal, creating localized domain. This process has been originally demonstrated by illuminating various ferroelectrics such as  $\text{LiNbO}_3$  and SBN with UV light.<sup>[18]</sup> We showed previously that the same mechanism can be employed to invert domains in the bulk of the ferroelectric multi- and single-domain crystal by using ultrashort infrared (IR) laser beam.<sup>[14a]</sup> Unlike the UV illumination, the IR light almost does not experience linear absorption, and can be tightly focused anywhere inside the crystal. However, high intensity IR beam experiences nonlinear (multiphoton) absorption in the focal volume, leading to strong temperature gradient and subsequent thermoelectric field. Because the temperature gradient along the beam axis follows beam intensity distribution, domains can be inverted only in the half of the focal volume where the thermoelectric field opposes direction of spontaneous polarization (see Figure 5a). As the “primary” domains observed in our PMN-38PT crystal are clearly formed in the confined region near the focal volume, their formation is most likely governed by the presence of thermoelectric field. Since coercive field in PMN-38PT is  $8.25 \text{ kV cm}^{-1}$ ,<sup>[19]</sup> which is significantly less than in lithium niobate, formation of the isolated primary domains is expected to be easier than in other crystals.

Since the thermoelectric field is determined by the temperature gradient, its strength is directly proportional to the beam power. This explains why the “primary” domain reversal takes place after exceeding the threshold power (here 230 mW at 800 nm). For lower input power, the thermoelectric field is less than the coercive field and domains are not inverted.

As far as the “secondary” domains are concerned, our results suggest their formation involves contribution of space charge field to the pyroelectric field in the cooling stage of the domain writing process, which ultimately inverts spontaneous

polarization. Similar mechanism has been already reported in the literature in case of ferroelectrics subjected to heating and cooling cycles.<sup>[20]</sup> Assuming, for sake of argument, that the beam illuminates the sample from the  $-z$  surface, the process of domain inversion involves the following two stages.

When the laser beam is on, the nonlinear absorption of light results in heating of the focal region and formation of thermoelectric fields. The nonlinear absorption also leads to generation of free charge carriers (electrons/holes) excited either from valence band and/or defect centers, which are commonly present in various ferroelectrics and, particularly, in PMN-PT (see Figure 5b).<sup>[21]</sup> While outside the focus, the charges are also subject to pyroelectric field whose direction coincides with that of spontaneous polarization. The subsequent trapping of free charges on defects and resulting charge distribution are source of cylindrically symmetric space charge field with its polar component directed against the spontaneous polarization. Because of the bipolarity of thermoelectric field and unidirectional character of the pyroelectric field outside the focal region, the space charge field is expected to be stronger in the region above the focus.

When the laser beam is switched off, the crystal starts cooling down. This gives rise to increase of the spontaneous polarization and depolarizing field, while the screening and space charge fields remain practically unchanged (see Figure 5c). Subsequently, the net electric field in the region away from the beam is nonzero and its component along the polar axis is directed against the direction of spontaneous polarization vector. As this field is stronger in the region above the focus, it inverts spontaneous polarization in this region if its magnitude exceeds the coercive field (see Figure 5d). This leads to nucleation of the “secondary” domain and its subsequent growth toward the  $-z$  surface of the crystal. That is why the secondary domains grow only on the side of the focus which is closer to the  $-z$  surface of the crystal. Because of axial symmetry of the space charge field, these domains acquire a hollow cylinder-like shape. The power of the poling laser beam directly determines the concentration

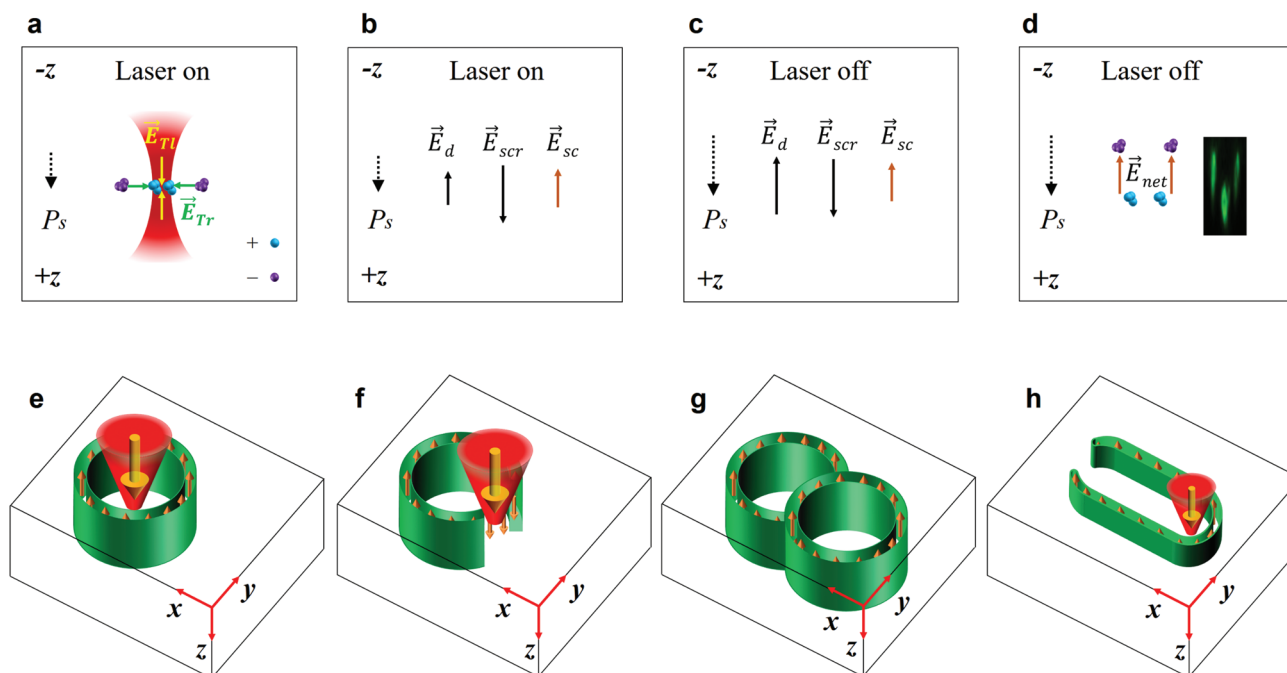


**Figure 5.** Illustrating mechanism of light-induced domain formation (top row) and erasure (bottom row) in PMN-38PT crystal. a) Formation of primary domains in the focal region. b–d) Formation of secondary domains outside of focal region: b) light excited charges migrate and after trapping form space charge field  $E_{sc}$ ; c–d) after the light is switched off the net electric field invert spontaneous polarization in the region closer to  $-z$  surface. The inset in (d) shows the recorded cross-section view of the primary and secondary domains in experiment.  $E_{Tl}$  and  $E_{Tr}$  represent the longitudinal and radial thermoelectric field, respectively.  $E_d$  and  $E_{scr}$  represent the depolarization field and screening field, respectively. e–g) Schematic diagram of the erasing process in writing domain patterns with period smaller than the diameter of the secondary domain. h) Formation of elongated-U-shaped domain pattern when the period of the pattern is small than  $2\ \mu\text{m}$ . The arrow in the focus of the beam indicates the laser induced thermoelectric field that erases previously formed secondary domain. The arrows at the domain area (green) indicate the direction of spontaneous polarization. The primary domains are omitted here for better illustration of the erasure process.

of charge carriers and, consequently, the strength of the space charge field. Hence, the secondary domains appear only after the beam power is high enough, which is 240 mW in the case depicted in Figure 3. Furthermore, the diameter and length of these domains strongly increase with beam power. Excited charges travel farther for higher power giving rise to larger diameter of the domains. In addition, as the local temperature increases with laser power, the subsequent cooling time increases as well enabling domains to grow longer.

The model discussed above assumes symmetry of the light-induced temperature distribution with respect to the focus. Consequently, it is insensitive to the direction of writing laser beam. However, our experiments show that the power threshold for the secondary domain inversion is slightly higher (10–15 mW) for the beam incident at the  $+z$  surface. This asymmetry is a consequence of the difference in the beam intensity distribution before and after the focus. There are two sources of this asymmetry. First, the very process of nonlinear absorption which leads to sharp intensity changes after the focus. Second, it is the optical birefringence which is known to deform the beam near its focus via so called focus splitting.<sup>[22]</sup> The net effect is that the light intensity distribution before and after the focus differ. As a result, the strength of thermoelectric fields generated by temperature gradient is no longer symmetric leading to difference in threshold power for domain inversion for beam arriving from different surfaces.

Graphs in Figure 5(e–h) illustrate schematically the discussed earlier optical erasure process shown in Figure 4. Since this process is independent of the time interval between forming two neighboring domains (see Figure S5 in the Supporting Information), the effect of space charge field generated during the nonequilibrium state can be excluded. Therefore, it is the light-induced thermoelectric field in the focal region that switches spontaneous polarization in the overlapping area of secondary domains. In the case of poling from  $-z$  surface, the direction of the thermoelectric field in the upper focal region opposes the direction of spontaneous polarization of the originally written secondary domain. Hence, this field erases the part of the preceding secondary domain (in the overlapping region) as the focus is translated to a new location, and a new secondary domain is formed. If the separation between writing locations is small enough, the adjacent secondary domains overlap so much that almost the whole area of the preceding domain can be inverted back. Subsequently, only the outmost right secondary domain survives and the elongated-U-shaped forms.

### 3. Conclusion

We demonstrated 3D domain inversions inside PT-relaxor-based single domain ferroelectrics utilizing IR femtosecond

laser pulses. This laser poling technique enables direct formation of localized 3D domains and their patterns inside monodomain PMN-38PT crystals. Two types of ferroelectric domains located either in the focus or outside of the beam could be simultaneously created depending on the laser beam power. The secondary domains can be erased by the subsequent poling beam providing the interval distance is small enough. All the laser induced domains remain stable for over two years at room temperature. A physical model was proposed to explain the generation and erasure of these domains.

These results are crucial for the applications utilizing domain inversions in PT-relaxor-based ferroelectrics. For the PT-relaxor-based ferroelectric crystals, whose excellent piezoelectric properties are intimately connected with the ferroelectric domain structures, the laser poling enables flexible domain patterning, and therefore can be used to optimize the electromechanical properties and explore the underlying physical mechanisms of the giant piezoelectricity. This makes the PT-relaxor-based ferroelectrics promising platform for developing the next generation hybrid devices combining the outstanding piezoelectric and optical effects in monolithic crystals.

## 4. Experimental Section

**Growth and Fabrication of Single-Domain PMN-38PT:** The tetragonal phase PMN-38PT crystal was grown via a modified Bridgman technique.<sup>[23]</sup> The crystal growth direction was [011]. The [001] direction of the single crystal was oriented by using the rotating orientation X-ray diffraction method.<sup>[24]</sup> The PT composition was deduced to be 38% by measuring the temperature dependence of dielectric permittivity of the crystal. The bulk single crystal was then diced into small plates (5×8×1 mm<sup>3</sup>), cutting perpendicular to the [001] direction with side cuts parallel to (010) and (100) planes. Before EFP, the (001) and (00 $\bar{1}$ ) faces of all plates were polished to optical grade. In order to avoid cracking in the subsequent electric field poling process, the crystals were annealed at 700 °C for 10 h, following by a slow cooling process with a temperate decreasing rate of 0.05–1 °C min<sup>-1</sup> near the Curie temperature. This slow cooling process can release the inner strains induced by crystal growth and mechanical treatment. Single-domain state was then successfully achieved by applying a 4 kV cm<sup>-1</sup> electric field along the [001] direction of the crystal in silicon oil at 140 °C. More details on single-domain fabrication can be found.<sup>[25]</sup> A polarized light microscope was used to verify the single-domain state (see Figure S1 in the Supporting Information for more details).

**Laser Poling in Single-Domain PMN-38PT:** To achieve ferroelectric domain inversion, a femtosecond oscillator (MIRA, Coherent) was used to generate laser pulses with a wavelength of 800 nm (in some experiment 780 nm), pulse duration of 180 fs and repetition rate of 76 MHz. The pulse energy of the laser beam can be continuously adjusted from 0 to 5 nJ by utilizing a half wave plate followed by polarizer. The laser beam with a selected power was then focused into the single domain crystal by a ×20 microscope objective (NA = 0.4). The crystal was mounted on a xyz-translation stage with stepper motor actuators. With a combination of the stage and an optical shutter, 3D ferroelectric domain structures could be inscribed, starting from the deepest level, and going up toward the surface of the crystal. The pulse energy was used for writing domain structure in Figures 1–4 is 3.3 nJ.

The optically poled domain patterns are barely visible under optical microscope. To facilitate locating the optically poled domain structures, a pulse energy of 3.7 nJ was used to write certain marks nearby, which consist of damaged spots.

In addition to the ĆSHM, the laser induced domains were also characterized using the piezoresponse force microscopy (PFM).

To this end, the sample was polished slightly to expose the laser induced domains for PFM measurement. The results show clearly the phase difference of 180° between the laser-processed and pristine areas, confirming the inversion of the spontaneous polarization and ferroelectric domains formation.

## Supporting Information

Supporting Information is available from the Wiley Online Library or from the author.

## Acknowledgements

This work was supported by the National Natural Science Foundation of China (Grant Nos. 11904273, 11974196, and 61675158), Research Start-up Program of Xidian University (Grant No. 10251180017), Yongjiang Scholar Foundation of Ningbo, the Qatar National Research Program (Grant No. NPRP 12S-0205-190047) and the Australian Research Council. The authors acknowledge support from the Centre for Advanced Microscopy, Australian National University and Dr. Jie Tian from MicroNano Research Facility, Royal Melbourne Institute of Technology University.

## Conflict of Interest

The authors declare no conflict of interest.

## Data Availability Statement

The data that support the findings of this study are available from the corresponding author upon reasonable request.

## Keywords

all-optical poling, ferroelectric domain erasure, PMN-PT, relaxor ferroelectrics

Received: October 1, 2021

Revised: November 19, 2021

Published online: December 19, 2021

- [1] a) S. E. Park, T. R. Shrout, *J. Appl. Phys.* **1997**, *82*, 1804; b) R. F. Service, *Science* **1997**, *275*, 1878; c) Z. G. Ye, *MRS Bull.* **2009**, *34*, 277; d) S. Zhang, F. Li, *J. Appl. Phys.* **2012**, *111*, 2. e) E. Sun, W. Cao, *Prog. Mater. Sci.* **2014**, *65*, 124; f) Y. Wang, Z. Wang, W. Ge, C. Luo, J. Li, D. Viehland, J. Chen, H. Luo, *Phys. Rev. B* **2014**, *90*, 134107; g) F. Li, D. Lin, Z. Chen, Z. Cheng, J. Wang, C. Li, Z. Xu, Q. Huang, X. Liao, L. Q. Chen, *Nat. Mater.* **2018**, *17*, 349; h) C. Qiu, B. Wang, N. Zhang, S. Zhang, J. Liu, D. Walker, Y. Wang, H. Tian, T. R. Shrout, Z. Xu, *Nature* **2020**, *577*, 350.
- [2] a) Y. Lu, Z. Y. Cheng, Y. Barad, Q. M. Zhang, *J. Appl. Phys.* **2001**, *89*, 5075; b) F. Wu, B. Yang, E. Sun, G. Liu, H. Tian, W. Cao, *J. Appl. Phys.* **2013**, *114*, 027021; c) C. Deng, L. Ye, C. He, G. Xu, Q. Zhai, H. Luo, Y. Liu, A. J. Bell, *Adv. Mater.* **2021**, *33*, 2103013.
- [3] Y. Zhao, X. Liu, B. Li, Q. Hu, Y. Zhuang, X. Fu, P. Luan, W. Zhao, Y. Liu, Z. Li, *Ferroelectrics* **2019**, *542*, 112.
- [4] a) Y. Q. Lu, Y. Y. Zhu, Y. F. Chen, S. N. Zhu, N. B. Ming, Y. J. Feng, *Science* **1999**, *284*, 1822; b) D. Yudin, S. Benchabane, D. Janner,

- V. Pruneri, *Appl. Phys. Lett.* **2009**, *95*, 052901; c) D. Yulistira, A. Boes, B. Djafari-Rouhani, Y. Pennec, L. Yeo, A. Mitchell, J. Friend, *Phys. Rev. Lett.* **2014**, *113*, 215503.
- [5] a) Z. Liu, X. Zhang, Y. Mao, Y. Zhu, Z. Yang, C. T. Chan, P. Sheng, *Science* **2000**, *289*, 1734; b) T. Still, W. Cheng, M. Retsch, R. Sainidou, J. Wang, U. Jonas, N. Stefanou, G. Fytas, *Phys. Rev. Lett.* **2008**, *100*, 194301; c) F. Lemoult, N. Kaina, M. Fink, G. Lerosey, *Nat. Phys.* **2013**, *9*, 55; d) E. Alonso-Redondo, M. Schmitt, Z. Urbach, C. Hui, R. Sainidou, P. Rembert, K. Matyjaszewski, M. Bockstaller, G. Fytas, *Nat. Commun.* **2015**, *6*, 8309.
- [6] D. Yulistira, A. Boes, A. R. Rezk, L. Y. Yeo, J. R. Friend, A. Mitchell, *Adv. Mater. Interfaces* **2014**, *1*, 1400006.
- [7] a) V. Berger, *Phys. Rev. Lett.* **1998**, *81*, 4136; b) N. Broderick, G. Ross, H. Offerhaus, D. Richardson, D. Hanna, *Phys. Rev. Lett.* **2000**, *84*, 4345; c) A. Arie, N. Voloch, *Laser Photonics Rev.* **2010**, *4*, 355.
- [8] J. A. Armstrong, N. Bloembergen, J. Ducuing, P. Pershan, *Phys. Rev.* **1962**, *127*, 1918.
- [9] S. Matsumoto, E. Lim, H. Hertz, M. Fejer, *Electron. Lett.* **1991**, *27*, 2040.
- [10] F. Li, L. Wang, L. Jin, Z. Xu, S. Zhang, *CrystEngComm* **2014**, *16*, 2892.
- [11] a) A. D. Ushakov, A. A. Esin, A. R. Akhmatkhanov, Q. Hu, X. Liu, Y. Zhao, X. Wei, V. Ya. Shur, *Appl. Phys. Lett.* **2018**, *113*, 112902; b) X. Liu, Y. Zhao, Q. Hu, A. D. Ushakov, P. Luan, X. Fu, W. Zhao, Y. Zhuang, A. R. Akhmatkhanov, V. Ya. Shur, Y. Liu, Z. Li, X. Wei, Z. Xu, *J. Eur. Ceram. Soc.* **2020**, *40*, 2922.
- [12] P. Zelenovskiy, E. Greshnyakov, D. Chezganov, L. Gimadeeva, E. Vlasov, Q. Hu, X. Wei, V. Shur, *Crystals* **2019**, *9*, 65.
- [13] a) T. Xu, K. Switkowski, X. Chen, S. Liu, K. Koynov, H. Yu, H. Zhang, J. Wang, Y. Sheng, W. Krolikowski, *Nat. Photonics* **2018**, *12*, 591; b) S. Liu, K. Switkowski, C. Xu, J. Tian, B. Wang, P. Lu, W. Krolikowski, Y. Sheng, *Nat. Commun.* **2019**, *10*, 3208.
- [14] a) X. Chen, P. Karpinski, V. Shvedov, K. Koynov, B. Wang, J. Trull, C. Cojocar, W. Krolikowski, Y. Sheng, *Appl. Phys. Lett.* **2015**, *107*, 141102; b) X. Chen, P. Karpinski, V. Shvedov, A. Boes, A. Mitchell, W. Krolikowski, Y. Sheng, *Opt. Lett.* **2016**, *41*, 2410.
- [15] B. Wang, X. Hong, K. Wang, X. Chen, S. Liu, W. Krolikowski, P. Lu, Y. Sheng, *Nanoscale* **2021**, *13*, 2693.
- [16] L. M. Mazur, S. Liu, X. Chen, W. Krolikowski, Y. Sheng, *Laser Photonics Rev.* **2021**, *15*, 2100088.
- [17] Y. Sheng, A. Best, H. J. Butt, W. Krolikowski, A. Arie, K. Koynov, *Opt. Express* **2010**, *18*, 16539.
- [18] a) A. Muir, C. Sones, S. Mailis, R. Eason, T. Jungk, Á. Hoffmann, E. Soergel, *Opt. Express* **2008**, *16*, 2336; b) A. Boes, T. Crasto, H. Steigerwald, S. Wade, J. Frohnhaus, E. Soergel, A. Mitchell, *Appl. Phys. Lett.* **2013**, *103*, 142904.
- [19] H. Cao, B. Fang, H. Xu, H. Luo, *Mater. Res. Bull.* **2002**, *37*, 2135.
- [20] a) V. Y. Shur, D. Kuznetsov, E. Mingaliev, E. Yakunina, A. Lobov, A. Ievlev, *Appl. Phys. Lett.* **2011**, *99*, 082901; b) V. Y. Shur, M. Kosobokov, E. Mingaliev, V. Karpov, *AIP Adv.* **2015**, *5*, 107110; c) J. Imbrock, H. Hanafi, M. Ayoub, C. Denz, *Appl. Phys. Lett.* **2018**, *113*, 252901.
- [21] C. He, Z. Zhou, D. Liu, X. Zhao, H. Luo, *Appl. Phys. Lett.* **2006**, *89*, 261111.
- [22] G. Zhou, A. Jesacher, M. Booth, T. Wilson, A. Ródenas, D. Jaque, M. Gu, *Opt. Express* **2009**, *17*, 17970.
- [23] S. Zhang, J. Luo, W. Hackenberger, T. R. Shrout, *J. Appl. Phys.* **2008**, *104*, 064106.
- [24] F. Li, L. Jin, Z. Xu, Z. Guo, *Rev. Sci. Instrum.* **2009**, *80*, 085106.
- [25] Y. Zhao, S. Wang, X. Fu, Y. Zhuang, R. Yang, Z. Yang, Z. Li, Z. Xu, X. Wei, *J. Appl. Phys.* **2018**, *123*, 084104.